AUTOMATIC FOREST AREA EXTRACTION FROM IMAGING SPECTROSCOPY DATA USING AN EXTENDED NDVI

Fabian Faßnacht[1], Holger Weinacker[2] and Barbara Koch[3]

1. University of Freiburg, Department FELIS, Freiburg, Germany; fabian.fassnacht@felis.uni-freiburg.de
2. University of Freiburg, Department FELIS, Freiburg, Germany; holger.weinacker@felis.uni-freiburg.de
3. University of Freiburg, Department FELIS, Freiburg, Germany; barbara.koch@felis.uni-freiburg.de

ABSTRACT

A method is presented to automatically extract tree-covered areas from airborne and simulated spaceborne imaging spectroscopy data. The method is based on the extended Normalized Difference Vegetation Index (NDVI).

The function of the index is to continuously decrease the index-values of all land surface classes in relation to the reflection values of tree-covered areas resulting in an index image with tree covered areas having highest values. Besides the typical wavelengths of the NDVI in the visual red and the near infrared section of the spectrum (660nm & 760 nm) two additional channels in the near infrared (810nm & 2450nm) were selected to boost the NDVI. Mean reflectance values of different land use surface classes were used to scale and weight the reflectance values within the selected channels resulting in values similar to the outcome of the NDVI (values from -1 to 1).

Based on the calculated index-image and an additional variance-image derived from the index-image a binary mask was created using a threshold value for each of the input images.

The method was applied to 19 HyMap-Scenes with ground sampling distances (GSD) varying between 4m and 8m. Additionally the index was tested on a simulated EnMAP scene with 30m GSD. After calibrating the index to the sensor by including the mean reflectance values of only a few training areas collected in two HyMap-scenes the method delivered promising results over all 19 HyMap scenes collected in various regions of Germany. For usage with the simulated EnMAP scene the threshold value of the variance image had to be adapted. Forest / non-forest classification accuracies of four statistically evaluated scenes reached from 92.0% to 96.6%. Almost all misclassified samples could be assigned to one of the following three classes: 1. Areas influenced by BRDF effects at the border of the image or in pronounced terrain situations 2. Swampy areas 3. Agricultural areas (esp. maize).

INTRODUCTION

Forests play a major role in the world's terrestrial ecosystems as well as in worldwide climatic processes. Forest ecosystems provide a wide range of material and nonmaterial benefits such as wood, fibre, game, pharmaceutical usable herbs, oxygen production, carbon absorption, habitat, erosion protection and many more. To protect and sustain forests as an efficient source of the aforementioned benefits, sustainable management practices and the reduction of deforestation and forest degradation has to be in the focus of forestry practitioners and researchers. Worldwide activities such as the United Nations Collaborative Programme on Reducing Emissions from Deforestation and Forest Degradation in Developing Countries (REDD) reflect the worldwide awareness of this important issue.

Remote Sensing with its ability to collect continuous data over wide areas is an important tool in assessing the actual state of worldwide forests and can be used as an efficient source of information on local, regional and global scale.

After the successful collection and calibration of airborne or spaceborne remote sensing data an important first step for all interest groups working with forests is to separate forested areas from other land use surfaces. In the last two decades several methods aiming on forest / non forest classification have been presented. The approaches based on a variety of sensors including radar (1,2), optical (3,4,5,6,7), lidar (8) as well as combined lidar / optical approaches (9).

Studies based on Imaging Spectroscopy were in the past rather focusing on the extraction of more complex information such as tree species (16, 17), biomass (18), chlorophyll content (15), etc. than on basic forest / non-forest classifications. Nevertheless the increased spectral information provided by imaging spectroscopy data has a very high potential to enhance classification results compared to results originating from other optical data sources.

The work presented here is part of the project ForestHype that is conducted in the framework of the German EO mission EnMap (10). Main goals of ForestHype are the development of methods for the future EnMAP sensor aiming on above ground biomass estimation, stress detection and derivation of biochemical and biophysical parameters within middle European forests. The automatic extraction of forested areas from hyperspectral HyMap and simulated EnMAP images is a first step to reach those goals. Therefore in this study we suggest a fast and efficient method for automatic retrieval of tree covered areas from hyperspectral images. One of the main goals within the study was to avoid standard classification algorithms from the field of machine learning such as Maximum Likelihood, Support Vector Machine, etc. since these methods often involve drawbacks such as the definition of new training areas for each image, long processing times and lack of transferability. This is especially true for highly collinear hyperspectral data. Instead we were aiming on a simple index-based method that makes direct use of the increased spectral information of imaging spectroscopy data and at the same time avoids potential problems due to the collinearity of hyperspectral data by only incorporating some selected bands. Based on this index and an additional variance image calculated from the index image a binary mask representing forest and non-forest areas was retrieved.

METHODS

Test sites

The test site is a managed forest located in the northern part of Karlsruhe, in the state of Baden-Württemberg (BW), South Western Germany. The area covers more than 900 ha of forest stands dominated by Pine, Oak and Beech. Exact species composition is listed in Table 1. The composition is contrasting with the average forest conditions in BW, where Spruce (Picea abies) is the dominating tree species (11).

Besides the main test site in Karlsruhe which was also used for the calibration of the index we evaluated the method on two other test sites located in Northeim, central Germany close to Hannover and in the Alpine Foreland close to Munich. For both of these sites no detailed tree species information was available.

Remote Sensing data

HyMap images

In August 2010 two HyMap images were acquired over the test site in Karlsruhe during the HyEurope campaign of the German Aerospace Research Centre and Space Agency (DLR). The sensor delivered imagery with 125 channels with wavelengths reaching from 0.45 to 2.48 µm. The spectral resolution of the channels varies from 13 – 17nm. The data were collected in two strips with a ground sampling distance (GSD) of 4m and 8m. Both strips were atmospherically and geometrically correct by DLR using ATCOR4 model and ORTHO software.

Additional 19 HyMap-Images with similar properties from the HyEurope campaign 2009 were available for further evaluation. One of these images – Northeim – was selected for further evaluation. The scene was mainly selected since it showed a well-balanced ratio of forested and non for-

ested areas in combination with a rather small extent, which alleviated the collection of reference data.

Table 1: Tree species composition of the study site (source: forest management plan)

Tree Species	**Percentage of forest area**		
Scotch pine (Pinus sylvestris)	51%	Douglas fir (Pseudotsuga menziesii)	5%
Oak (Quercus petraea)	14%	Hornbeam (Carpinus betulus)	4%
Beech (Fagus sylvatica)	10%	Other species	6%
Red Oak (Quercus rubra)	10%		

Simulated EnMAP images

Besides the aforementioned airborne HyMap images the index proposed in this study was also applied to a simulated spaceborne EnMAP scene with 30m GSD. In the framework of the EnMAP space mission an approach for the simulation of EnMAP scenes was developed. At the German Research Centre for Geosciences (GFZ) an EnMAP scene simulator consisting of five sequential processing modules was designed. The modules include 1. a reflectance module, 2. a spatial module, 3. an atmospheric module, 4. a spectral module and 5. a radiometric module. This "EnMAP scene simulator is able to generate realistic EnMAP-like data in an automatic way under a set of user-driven instrumental and scene parameters" (12).

The simulated EnMAP scene over the Munich alpine foreland in Southern Germany was derived from a Landsat-TM image using SLC model (13) and the EnMAP scene simulator of GFZ.

Reference Data

For each of the three test sites that were used to statistically evaluate the proposed method a reference dataset was created. Therefore a regularly spaced grid was projected onto the scenes and each of the crossing points of the grid was classified as forest or non forest sample point. For three of the four images (2 images from the test site in Karlsruhe, one in Northeim) where no land use reference data was available this classification was performed by visual interpretation of True Color and Color Infrared composites of HyMap images with 4m GSD. Samples that could not be identified as forest or non forest with a very high probability were deleted from the reference data set. For the simulated EnMAP scene "alpine foreland" with 30m GSD a land cover reference data set was available and the samples were classified based on this reference. Table 2 lists the number of samples and grid spacing distance for each of the test sites. For the test site in Karlsruhe only one reference dataset was created and used for both images. Therefore in the scene with 8m resolution only the part of the scene overlapping with the 4m scene was evaluated. The slightly varying number of samples is due to non-overlapping parts of the two scenes.

Table 2: Number of reference samples of the five test sites used to evaluate the FABI

Test site	***Number of samples***	***samples classified as forest***	***samples classified as non forest***
Karlsruhe (4m GSD) – HyMap; Grid spacing: 20m	54100	38235	15865
Karlsruhe (8m GSD) – HyMap; Grid spacing: 20m	50845	35745	15100
Northeim (4m GSD) – HyMap; Grid spacing: 20m	35252	16825	18427
Alpine foreland (30m GSD) – simulated EnMAP; Grid spacing: 65m	212521	69194	143327

Forest Area Boost Index (FABI)

The main advantage of hyperspectral data over multispectral and other optical data is the increased spectral resolution. In this study we assume that it is possible to separate forested areas from all other land use surfaces using only a few narrow reflectance values of key wavelengths. The proposed Forest Area Boost Index (FABI) bases on the NDVI. The NDVI was first formulated by Rouse et al. (14) as the normalized ratio between NIR and red reflectance. The NDVI uses the information of the red edge - a phenomena that describes the rapid increase of reflectance of vegetation from the visual red to the NIR section of the light due to the change from strong chlorophyll absorption in the red to strong scattering of light at the cell walls in the NIR region. NDVI values range from -1 to 1. Densely vegetated areas result in high NDVI values while soils show low and water bodies negative values. Thus NDVI is a useful tool to separate vegetated areas from other land use surfaces. However it is also reported that the NDVI fails in separating forests from other vegetation (2).

The initial idea of the FABI was to select additional wavelengths that have the potential to continuously increase reflectance values of forested areas compared to all other land use surfaces and combine these wavelengths with the NDVI. Therefore mean reflectance values over the full HyMap-spectrum were extracted for seven land use classes from two HyMap images with available ground truth data (Fig. 1). Reflectance values of each land use class were collected from multiple locations within the image to account for BRDF effects and natural variability.

Since the NDVI successfully separates vegetation from other land use classes the main task was to identify spectral regions that allow the separation between forests – in this study represented by two deciduous (oak – *Quercus petreae*, red oak – *Quercus rubra*) and one coniferous tree species (Pine – *Pinus sylvestris*) – and other vegetation represented by a sports field (representing brightest green vegetation) and maize (representing darkest green vegetation).

As illustrated in Fig. 1 a large part of the spectral curve of maize runs between the curves of deciduous and coniferous trees. Only HyMap channels 20 to 37 (~ 0.74 – 0.97 µm) show potential to separate maize from forested areas. Therefore channel 24 (~ 0.81) with the maximum difference between mean maize reflectance and mean forest reflectance (Oak) within this spectral range was selected. Since the reflectance curve of the sports field shows higher reflectance values than forests throughout the spectral range of the HyMap sensor channel 24 was supposed to boost the difference between forest reflectance and grassland reflectance represented by the sports field as well. Additionally Channel 21 (used to calculate the NDVI) was used a second time to further boost the difference between forested areas and grassland areas. Finally to enhance the difference between vegetation in general and urban areas as provided by NDVI HyMap channel 123 (~ 2.45 µm) was included. In this spectral region all reflectance curves of vegetation have similar reflectance values while urban areas show significantly higher values.

After the successful identification of spectral regions with potential to boost reflectance differences between forests and non forested areas the selected channels had to be implemented in an equation. The implementation had to fulfil two requirements: 1. The reflectance values had to be scaled to more or less synchronize with NDVI values 2. The synchronization should at the same time increase the potential of the final index image to separate forested and non forested areas.

As illustrated in Equation 1 mean reflectance values of selected land use classes were used to scale the reflectance values of the key wavelength selected in the step described before. In this study these mean reflectance values were extracted from two HyMap images and the values were rounded to full five hundreds. Table 3 lists the values used in Equation 1 in this study. These values may also be used in the case of lacking ground truth data.

Table 3: Rounded mean reflectance values used in Equation 1.

Land use class / wavelength	**Rounded Reflectance values**
$MeanRefl_{Urban\ 660nm}$	1000
$MeanRefl_{Urban\ 810nm}$	1500
$MeanRefl_{Urban\ 2450nm}$	1500
$MeanRefl_{DecForests\ 810nm}$	3000

An example will lead to a deeper understanding of the developed method to meet the two requirements explained above: In Part 3 of the FABI (Equation 2) the mean reflectance of urban areas is subtracted from the reflectance value of each pixel and the result is divided by the mean reflectance value of deciduous forests. The subtraction of the mean urban reflectance leads to an exclusion of urban areas from the boost effect of this part of the FABI since the numerator will have values of +-0 for urban pixels. At the same time the relative difference between maize (and grass land) and forest is increasing (Fig. 1). Due to the subtraction of the mean urban reflectance values the results of this part of the FABI would be negative for water bodies and therefore increase the overall FABI-value for water. Since this would hamper the separation of water bodies from forest the absolute value of part 3 of the FABI is used in the further calculation. The adjacent division by the mean reflectance value of deciduous forests scales the values to a similar range as the NDVI. Additionally the division has a weighting effect: The smaller the denominator is the larger is the influence of this part of the FABI.

$$\frac{Refl_{\mathbf{760nm}} - Refl_{\mathbf{660nm}}}{Refl_{\mathbf{760nm}} + Refl_{\mathbf{660nm}}} - \frac{Refl_{\mathbf{660nm}}}{MeanRefl_{Urban\ \mathbf{660nm}}} - \left|\frac{Refl_{\mathbf{810nm}} - MeanRefl_{Urban\ \mathbf{810nm}}}{MeanRefl_{DecForests\mathbf{810nm}}}\right| - \frac{Refl_{\mathbf{2450nm}}}{MeanRefl_{Urban\ \mathbf{2450nm}}}$$

(Equation 1)

$$\left|\frac{Refl_{\mathbf{810nm}} - MeanRefl_{Urban\ \mathbf{810nm}}}{MeanRefl_{DecForests\mathbf{810nm}}}\right|$$

(Equation 2)

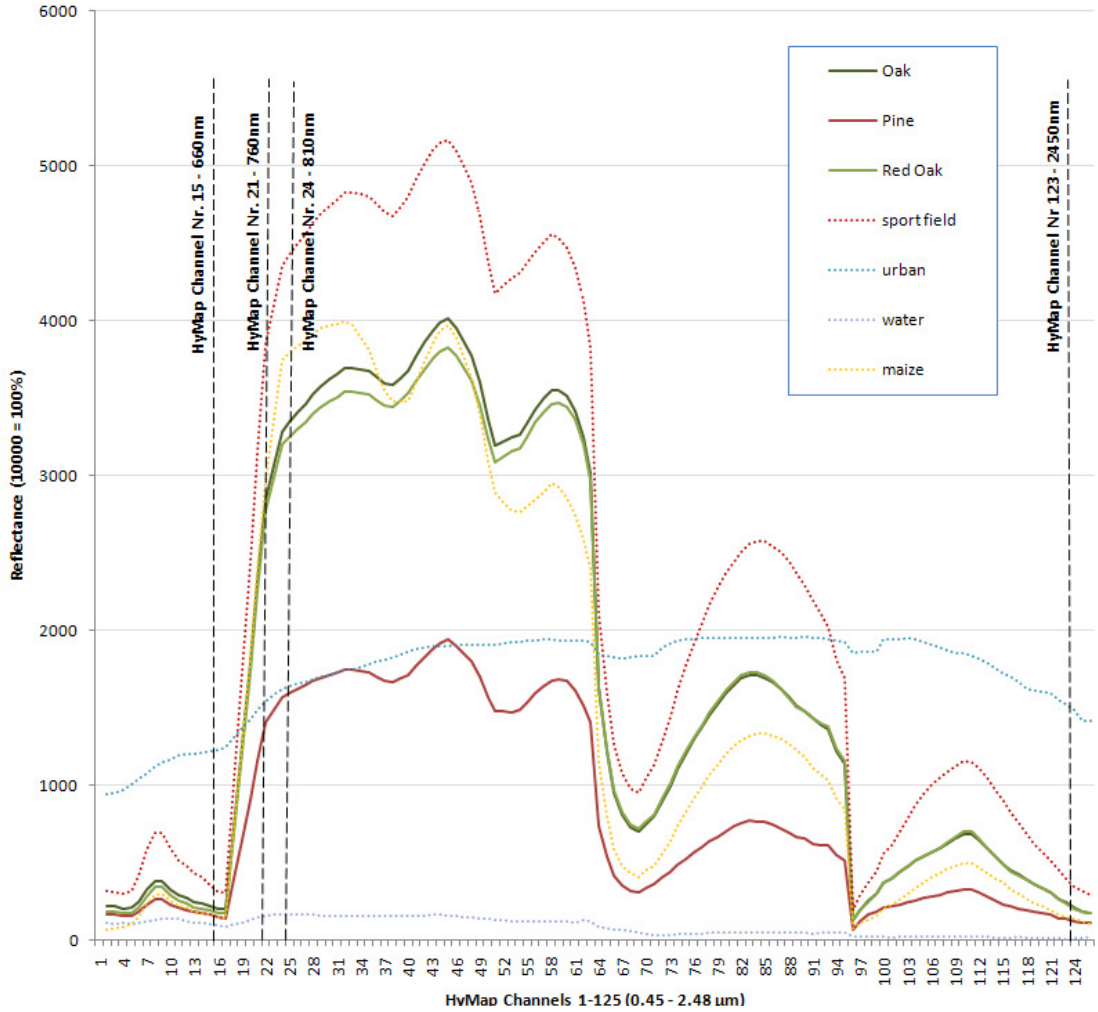

Fig.1: Mean reflectance values extracted from seven land use classes and plotted against the wavelength. All reflectance curves representing forests are plotted with solid lines, other land use classes are plotted with dashed line. Wavelengths used in the FABI are marked with vertical black lines.

To further clarify the function of the index equation 1 can be divided into four parts: Part 1 is represented by the NDVI and Part 2-4 mirror the implemented boost channels. The functionality of part 2-4 is best described using an example: Table 4 lists typical reflectance values of the 7 land use classes illustrated in Fig. 1 at the specific wavelengths used in the FABI. Table 5 lists the results for the four parts of the FABI calculated based on those values. The comparison between the hard separable land use classes oak and maize (marked in Table 5) will explain the function of the FABI: The NDVI value of maize (0.851) in the example is larger than the NDVI value of Pine (0.810) and only slightly less than the NDVI value of Oak (0.868). The goal of the FABI is to continuously increase the values for forested areas in comparison to other land use surfaces. Since parts 2-4 of the FABI will be subtracted from the original NDVI values (Equation 1) the values of the individual parts of the FABI have to be larger for maize than for Oak. This is in this example true for parts 2-4 of the FABI. The largest difference can be observed in part 3. This part was designed to separate grassland and other green vegetation from forested areas and their functionality is thus confirmed in this example. In some cases grass land and crops might have slightly lower values than forests in Parts 2 and 4. Since Part 2 and 4 have a significant positive effect in enhancing the difference of vegetation in general and urban areas they are still accepted as part of the FABI. After subtracting Parts 2-4 from the original NDVI values the class maize has significantly lower FABI values (-0.294) than the class Oak (-0.085) and the other two forestry classes used in

this example (-0.008 (Red Oak), 0.552 (Pine)). As illustrated in table 4 the three remaining land use classes sports field (-0.666), water (-0.712) and urban areas (-2.156) also show considerably smaller FABI-values than the three forest classes.

Table 4: Reflectance values of seven land use classes at the seven wavelengths used in the FABI.

	Pine	*Oak*	*Red Oak*	*sports field*	*urban*	*water*	*maize*
$Refl_{660\ nm}$	147	200	173	312	1232	48	243
$Refl_{760\ nm}$	1407	2846	2773	3855	1545	34	3024
$Refl_{810\ nm}$	1597	3345	3247	4424	1640	33	3734
$Refl_{2450\ nm}$	119	208	203	345	1485	7	237

Table 5: Individual results for the four parts of the FABI based on the values of Table 3.

	Pine	*Oak*	*Red Oak*	*sports field*	*urban*	*water*	*maize*
Part 1 $\frac{Refl_{760nm} - Refl_{660nm}}{Refl_{760nm} + Refl_{660nm}}$ ***(NDVI)***	0.810	0.868	0.882	0.850	0.112	-0.171	0.851
Part 2 $\frac{Refl_{660nm}}{MeanRefl_{Urban\ 660nm}}$	0.147	0.2	0.173	0.312	1.232	0.048	0.243
Part 3 $\left\lvert\frac{Refl_{810nm} - MeanRefl_{Urban\ 810nm}}{MeanRefl_{DecForests\ 810nm}}\right\rvert$	0.0323	0.615	0.582	0.974	0.046	0.489	0.745
Part 4 $\frac{Refl_{2450nm}}{MeanRefl_{Urban\ 2450nm}}$	0.079	0.138	0.135	0.23	0.99	0.005	0.158
FABI - Value	0.552	-0.085	-0.008	-0.666	-2.156	-0.712	-0.294

Calculation of the final forest/non forest mask

For the calculation of the forest / non forest mask the FABI-image and an additional variance image calculated from the FABI-image were used as input. The variance image is calculated from a 3 x 3 neighbourhood of each pixel in the index-image. The variance image was implemented since some agricultural areas with very similar spectral behaviour as forests were not separable by the FABI alone. However the variance of the FABI in agricultural areas is significantly lower than in most forested areas and the implementation of a variance image is therefore an effective method to exclude most of these areas from the forest class.

Subsequently the decision whether a pixel is classified as forest or non-forest depends upon two different threshold values. 1. Threshold value for FABI values 2. Threshold value for the variance image values. The threshold values were defined after analyzing the histograms of the input images. Regarding the threshold value for the variance image it was not possible to use a fixed threshold for all scenes since the variance in general decreases with lower spatial resolution. Hence two threshold values were used within this study – one for all images with 4m and 8m GSD and a second for the scene with 30m GSD.

Application of a 3 x 3 median filter smoothed results of the outcome binary mask and improved results for the images with higher spatial resolution.

RESULTS

Forest mask accuracies

Tables 5-12 show confusion matrices for four evaluated scenes – each scene was evaluated as delivered from the classification procedure and additionally after applying a 3x3 median filter. Overall accuracies were lowest at the test site in Karlsruhe (4m GSD, no median filter) and highest at the Alpine foreland scene (30m GSD, no median filter) reaching 92.01 % and 96.65 % respectively. The user's accuracy for the forest class is in all cases higher than the user`s accuracy for the non forest class reaching a maximum of 99.69 % in the Northeim test site (no median filter) and a minimum of 95.16 % in the Alpine foreland test site image (with 3x3 median filter). The user`s accuracies for the non forest class range from 80.68 % at the 4m GSD image of Karlsruhe to 96.29 % in the Alpine foreland test site (no median filter). Producer`s accuracies vary from test site to test site and unlike as in the user's accuracies none of the classes showed significantly higher values than the other if all images are considered. Highest producer`s accuracies were found for the non forest class in the Northeim test site (99.44 %) while lowest values (86.88 %) were found for the forest class in the same image. The application of a 3 x 3 median filter improved overall accuracies of all images with 4m and 8m GSD (maximum improvement from 92.01% to 95.08% (3.07 % difference) at the test site in Karlsruhe, 4m GSD) while for the 30m GSD images the overall accuracy decreased with application of the filter.

Misclassification of forest samples mainly occurred due to BRDF effects at the borders of HyMap images or due to too low variance values in very dense stands with homogenous and closed canopies. Misclassified non forest samples mostly belonged to wet vegetated areas such as swamps and marshlands or to maize.

Table 5: Confusion matrix – test site Karlsruhe, 4m GSD, binary mask

	Samples Forest (reference data)	***Samples non forest (reference data)***	***Sum***	***User`s accuracy***
Classified as Forest	34599	685	35284	98.1 %
Classified as non forest	3636	15180	18816	80.68 %
Sum	38235	15865	54100	**Overall accuracy**
Producer`s accuracy	90.49 %	95.68 %		92.01 %

Table 6: Confusion matrix – test site Karlsruhe, 4m GSD, binary mask, 3 x 3 median filter

	Samples Forest (reference data)	***Samples non forest (reference data)***	***sum***	***User`s accuracy***
Classified as Forest	36027	452	36479	98.76 %
Classified as non forest	2208	15413	17621	87.47 %
Sum	38235	15865	54100	**Overall accuracy**
Producer`s accuracy	94.23 %	97.15 %		95.08 %

Table 7: Confusion matrix – test site Northeim, 4m GSD, binary mask

	Samples Forest (reference data)	***Samples non forest (reference data)***	***sum***	***User`s accuracy***
Classified as Forest	14617	45	14662	99.69 %
Classified as non forest	2208	18382	20590	89.28 %
Sum	16825	18427	35252	**Overall accuracy**
Producer`s accuracy	86.88 %	99.76 %		93.61 %

Table 8: Confusion matrix – test site Northeim, 4m GSD, binary mask, 3 x 3 median filter

	Samples Forest (reference data)	***Samples non forest (reference data)***	***sum***	***User`s accuracy***
Classified as Forest	15274	104	15378	99.32 %
Classified as non forest	1551	18323	19874	92.20 %
Sum	16825	18427	35252	**Overall accuracy**
Producer`s accuracy	90.78 %	99.44 %		95.31 %

Table 9: Confusion matrix – test site Karlsruhe, 8m GSD, binary mask

	Samples Forest (reference data)	***Samples non forest (reference data)***	***sum***	***User`s accuracy***
Classified as Forest	33934	1462	35396	95.87 %
Classified as non forest	1811	13638	15449	88.28 %
Sum	35745	15100	50845	**Overall accuracy**
Producer`s accuracy	94.93 %	90.32 %		93.56 %

Table 10: Confusion matrix – test site Karlsruhe, 8m GSD, binary mask, 3 x 3 median filter

	Samples Forest (reference data)	***Samples non forest (reference data)***	***sum***	***User`s accuracy***
Classified as Forest	34566	1104	35670	96.90 %
Classified as non forest	1179	13996	15175	92.23 %
Sum	35745	15100	50845	**Overall accuracy**
Producer`s accuracy	96.70 %	92.69 %		95.51 %

Table 11: Confusion matrix – test site Alpine foreland, 30m GSD, binary mask

	Samples Forest (reference data)	***Samples non forest (reference data)***	***sum***	***User`s accuracy***
Classified as Forest	63743	1667	65410	97.45 %
Classified as non forest	5451	141660	147111	96.29 %
Sum	69194	143327	212521	**Overall accuracy**
Producer`s accuracy	92.12 %	98.84 %		96.65 %

Table 12: Confusion matrix – test site Alpine foreland, 30m GSD, binary mask, 3 x 3 median filter

	Samples Forest (reference data)	***Samples non forest (reference data)***	***sum***	***User`s accuracy***
Classified as Forest	61325	3122	64447	95.16 %
Classified as non forest	7869	140205	148074	94.69 %
Sum	69194	143327	212521	**Overall accuracy**
Producer`s accuracy	88.63 %	97.82 %		94.83 %

CONCLUSIONS

The detection of forested areas from remote sensing data is an important task in a lot of scientific, environmental and governmental fields of application, especially taking into consideration that for climate purposes the correct mapping of forest land will gain significant importance worldwide. Although a number of methods working with various sensors were presented in the past, remote sensing is not commonly an integrated component of forest inventories (4). This might change with the rise of new hyperspectral spaceborne sensors which provide improved spectral information compared to traditional multispectral sensors and therefore have a high potential to increase the robustness and transferability of developed methods.

In this study a new index-based method for automatic forest area extraction from imaging spectroscopy data is presented. The proposed method avoids classical classification algorithms from the field of machine learning which results in slim processing times and the reduction of training samples. Evaluations of the methods with four scenes differing in spectral and spatial resolution resulted in high accuracies reaching from 92% to over 96%. The application of a 3 by 3 median filter improved classification results for all images with a GSD smaller than 8m. This can be explained by the fill up effect of the filter in small areas that were misclassified as non forest due to too low variance values. In this study a fix threshold value for the FABI Image was used in all four scenes. The implementation of an automatic retrieval of the threshold value based on the histogram of the FABI-Image might further improve classification results. Misclassification within wet areas could be addressed with the integration of an additional wetness index that allows the exclusion of wet areas before the forest classification procedure. The misclassifications of maize may be

avoided by moving the time of data acquisition to an earlier point of the growing season. Misclassified forest samples because of BRDF effects might be reduced with the help of pre-processing tools such as across-track illumination correction.

ACKNOWLEDGEMENTS

The authors are grateful to the German Aerospace Center and the German Federal Ministry of Economics and Technology for technical and financial support of this research.

REFERENCES

1 Zengyuan L, B Rosich & Erxue C, 1999. A Case Study of the Feasibility of Mapping Forest and Non-Forest using ILU Image Over Zengcheng Country in China. In: Proceedings of 20th Asican Conference on Remote Sensing, November 22-25, Hong Kong, China.

2 Ling F, Z Li, E Chen, Q Wang, 2009. Comparison of ALOS PALSAR RVI and Landsat TM NDVI for Forest Area Mapping. In: Proceedings 2nd Asian Pacisific COnferen on Synthetic Aperture Radar, Xian, Shanxi, China. pp. 132-135.

3 Rack J, 2000. Forest/Nonforest Classification of Landsat TM Data for Annual Inventory Phase One Stratification. Proceedings Second Annual Forest Inventory and Analysis (FIA) Symposium, Salt Lake City, UT, October 17-19, 2000.

4 Wynne R H, R G Oderwald, G A Reams & J A Scrivani 2000. Optical Remote Sensing for Forest Area Estimation: Journal of Forestry. 98(5): 31-36.

5 Wayman J P, R H Wynne, J A Scrivani & G A Reams, 2001. Landsat TM-based Forest Area Estimation Using Iterative Guided Spectral Class Rejection. ISPRS Photogrammetrc Engineering & Remote Sensing, 67 (10), pp. 1155-1166.

6 McRoberts R E, M D Nelson, D G Wendt, 2002. Stratified estimation of forest area using satellite imagery, inventory data, and the k-Nearest Neighbors technique. Remote Sensing of Environment, 82, pp. 457-468.

7 Haapanen R, A R Ek, M E Bauer, A O Finley, 2004. Delineation of forest/nonforest land use classes using nearest neighbor methods. Remote Sensing of Environment, 89, pp. 265-271.

8 Straub C, H Weinacker, B Koch, 2008. A fully automated procedure for delineation and classification of forest and non-forest vegetation based on full waveform laser scanner data. ISPRS Conference 2008 Beijing, Remote Sensing and Spatial Information Sciences, Vol. XXXVII. Part B8. Beijing 2008. pp. 1013 – 102

9 Wang Z, R Boesch, C Ginzler, 2008. Integration of high resolution aerial images and airborne lidar data for forest delineation. ISPRS Conference 2008 Beijing, Remote Sensing and Spatial Information Sciences, Vol. XXXVII. Part B8. Beijing 2008. pp. 1203 – 1207.

10 Stuffler T, C Kaufmann, S Hofer, K P Förster, G Schreier, A Mueller, A Eckhardt, H Bach, B Penne, U Benz & R Haydn, 2007. The EnMAP hyperspectral imager – An advanced optical payload for future applications in Earth observation programmes. Acta Astronautica, 61 (1-6), pp. 115-

11 Latifi H, A Nothdurft, B Koch, 2010. Non-parametric prediction and mapping of standing timber volume and biomass in a temperate forest: application of multiple optical/LiDAR-derived predictors. Forestry, 83 (4), pp.395 – 407.

12 Guanter L, K Segl, H Kaufmann, 2009. Simulation of Optical Remote-Sensing Scenes With Application to the EnMAP Hyperspectral mission. IEEE Transactions on Geoscience and Remote Sensing, 47 (7), pp.2340 – 2351.

13 Verhoef W, H Bach, 2003. Simulation of hyperspectral and directional radiance images using coupled biophysical and atmospheric RT-models. Remote Sensing of Environment, 87, pp. 23-41.

14 Rouse J, R Hass, J Schell, D Deering, 1973. Monitoring vegetation systems in the great plains with ERTS. Third ERTS Symposium 1973, NASA, SP-351 I, pp. 309-317.

15 Malenovský Z, C Ufer, Z. Lhotákova, J G P W Clevers, M E Schaepman, J Albrechtová, P Cudlín, 2006: A new hyperspectral index for chlorophyll estimation of a forest canopy: Area under curve normalised to maximal band depth between 650-725nm. EARSeL eProceedings 5, 2/2006, 161-172.

16 Apan A, S Phinn, T Maraseni, 2009: Discrimination of remnant tree species and regeneration stages in Queensland, Australia using hyperspectral imagery Hyperspectral Image and Signal Processing. First Workshop on Evolution in Remote Sensing, 2009. WHISPERS '09. 26-28 Aug. 2009 Page(s):1 – 4

17 Goodenough D G, A Dyk, G Hobart, Hao Chen, 2007: Forest information products from hyperspectral data — Victoria and Hoquiam test sites. Geoscience and Remote Sensing Symposium, 2007. IGARSS 2007. IEEE International 23-28 July 2007 Page(s):1532 – 1536.

18 Thenkabail P S, E A Enclona, M S Ashtin, C Legg, M J De Dieu, 2003: Hyperion, IKONOS, ALI, and ETM+ sensors in the study of African rainforests. Remote Sensing of Environment, 90, 23-43.